Synthesis and Characterization of Magnetically Modified Clay Composites

A. B. Bourlinos, M. A. Karakassides, A. Simopoulos, and D. Petridis*

Institute of Materials Science, NCSR "Demokritos", Ag. Paraskevi Attikis, Athens 153 10, Greece

Received February 16, 2000. Revised Manuscript Received June 8, 2000

The interaction of acetic acid vapors with iron-exchanged montmorillonites leads to iron acetate intercalates which upon pyrolysis transform to magnetic γ-iron oxide nanoparticles dispersed onto the external surface of the clay mineral. As these novel clay composites retain the original swelling and cation-exchange properties of the mineral, the synthesis of various clay derivatives is readily attained. X-ray diffraction, electron spin resonance, Mössbauer spectroscopy, magnetic measurements, and transmission electron microscopy provide evidence for the formation of magnetic iron oxide phase and also for its location in the clay structure.

Indroduction

Smectite clays, a class of layered aluminosilicate minerals, are endowed with unique swelling, intercalation, and ion-exchange properties that make them excellent materials for various industrial applications. Most attractive among clay derivatives are intercalated clay catalysts,[1,2] pillared clays,[3−5] clay−polymer composites,[6−9] activated clays as effective absorbents or fillers,[10] and clay coatings with diverse utilities.[11] Clay−nanocrystalline composites define another class of clay derivatives obtained from the uniform distribution of nanophase particles onto the clay surfaces. Semiconductors,[12,13] magnetic iron oxide nanoparticles,[14] and atomic clusters (Pd, Ru, Os)[15,16] are the main nanoscale partners in these clay composites. Clays modified with magnetic iron oxidic phases are promising materials for many important applications, such as in environment redemption,[17] magnetic separation of biochemical products,[18] and other biotechnological applications.[19,20]

In this paper we describe a novel method for the synthesis of magnetic clay composites consisting of magnetic iron oxide nanoparticles embedded onto the mineral surfaces. Remarkably, the magnetically modified clays retain their total cation-exchange capacity (CEC) as to the starting material, are easily redispersed in aqua media, and therefore can be converted to reconstructed clay derivatives, such as magnetic organo clays, pillared clays, clay−polymer composites, and others. In addition, the ability of swelling in aqueous media secures the formation of excellent magnetic clay films upon drying.

Experimental Section

Materials. The montmorillonite used in this study was from the island of Milos, Greece, with the code name Zenith-N and the following chemical composition:

$$Na_{0.63}K_{0.07}Ca_{0.11}\{Si_{7.75}Al_{0.25}\}\{Al_{3.21}Mg_{0.69}Fe^{3+}{}_{0.05}Ti_{0.05}\}O_{20}(OH)_4$$

The sample was fractionated to 2 μm by gravity sedimentation and purified by standard methods. The cation-exchange capacity of smectite is equal to 80 mequiv/100 g. For the iron-containing clay products the salt $FeCl_3 \cdot 6H_2O$ was used.

Synthesis of the Magnetic Clay Composites. A simple iron-exchanged clay was obtained as follows: To an aqueous suspension of 0.5 g of Na^+−montmorillonite in 25 mL of deionized water was added dropwise and under stirring 50 mL of an aqueous 0.02 M $FeCl_3 \cdot 6H_2O$ solution. The resulting mixture was stirred for 20 min, and then it was centrifuged and washed with water (3 × 50 mL), each time the mixture being stirred for 20 min. The intercalation procedure was repeated twice to secure a homoionic clay containing as possible similar oligonuclear iron species. Finally, the solid was redispersed into 20 mL of water and dried in air for 24 h by

* To whom correspondence should be addressed.

(1) Pinnavaia, T. J. *Science* **1983**, *220*, 365.
(2) Rupert, J. P.; Granquist, W. T.; Pinnavaia, T. J. In *Chemistry of Clays and Clay Minerals*; Newman, A. C. D., Ed.; Longman Scientific & Technical: Harlow, U.K., 1987; p 275.
(3) Mitchel, I. V. *Pillared Layered Structures. Current Trends and Applications*; Elsevier: London, 1990.
(4) Burch, R. *Catal. Today* **1988**, *2*, 1.
(5) Ohtsuka, K. *Chem. Mater.* **1997**, *9*, 2039.
(6) Legaly, G., Pinnavaia, T. J., Eds.; *Clay Mineral-Polymer Nanocomposites; Appl. Clay Sci.* **1999**, 15.
(7) Giannelis, E. P. *Adv. Mater.* **1996**, *8*, 29.
(8) Pinnavaia, T. J.; Lan, T.; Wang, Z.; Shi, H.; Kaviratna, P. D. *ACS Symp. Ser.* **1996**, *622*, 250.
(9) Aranda, P.; Ruiz-Hitzky, E. *Appl. Clay Sci.* **1999**, *15*, 119.
(10) Kirk, R. E., Othmer, D. F., Eds.; *Encyclopedia of Chemical Technology*; Interscience: New York, 1954; Vol. 4, pp 24−86.
(11) Nadeau, P. H. *Appl. Clay Sci.* **1987**, *2*, 83.
(12) Dékány, I.; Turi, L.; Tombácz, E.; Fendler, J. H. *Langmuir* **1995**, *11*, 2285.
(13) Dékány, I.; Turi, L.; Király, Z. *Appl. Clay Sci.* **1999**, *15*, 221.
(14) Skoutelas, A. P.; Karakassides, M. A.; Petridis, D. *Chem. Mater.* **1999**, *11*, 2754.
(15) Mastalir, A.; Notheisz, F.; Király, Z.; Bartók, M.; Dékány, I. *Stud. Surf. Catal.* **1997**, *108*, 477.
(16) Giannelis, E. P.; Pinnavaia, T. J. *Inorg. Chem.* **1985**, *24*, 3602.
(17) Navratil, J. D. In *Natural Microporous Materials in Environmental Technology*; Misaelides, P., Macášek, F., Pinnavaia, T. J., Colleda, C., Eds.; NATO Sci. Ser. E; Kluwer Acad. Pub.: Dordrecht, 1999; Vol. 362, p 417.
(18) Patton, W. F.; Kim, J.; Jacobson, B. S. *Biochim. Biophys. Acta* **1985**, *816*, 83.
(19) Penchev, I. P.; Hristov, J. Y. *Powder Technol.* **1990**, *61*, 103.
(20) Kemshead, J. T.; Treleaven, J. G.; Gibson, F. M.; Ugllstad, J.; Rembaum, A.; Philip, T. *Prog. Exp. Tumor Res.* **1985**, *29*, 249.

10.1021/cm000137o CCC: $19.00
Published on Web 08/09/2000

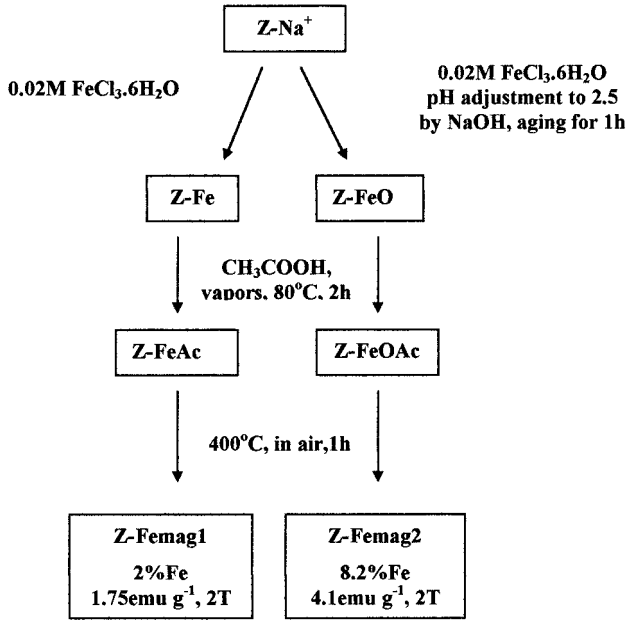

Figure 1. Synthetic pathways for the magnetic clay composites Z-Femag1 and Z-Femag2.

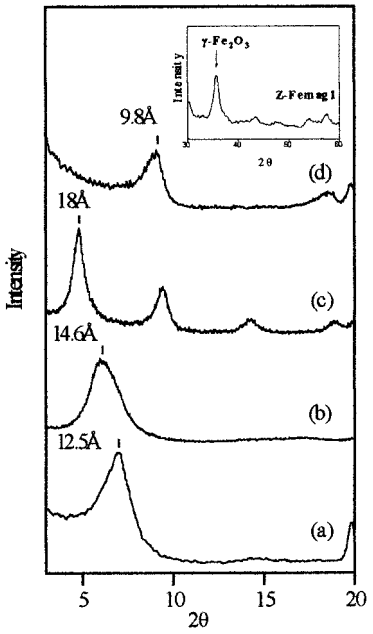

Figure 2. XRD patterns of (a) Z-Na, (b) Z-Fe, (c) Z-FeAc, and (d) Z-Femag1.

spreading over a glass plate. The dried sample was collected, crashed into a powder, and exposed to glacial acetic acid vapors in a small closed vessel for 2 h at 80 °C (Z-FeAc). After exposure, the sample was dried at the same temperature for few minutes in order to remove any surface-adsorbed acetic acid. The pale reddish powder was then placed in an nonsealed quartz tube (0.5 cm in diameter), and by calcination at 400 °C for 1 h in air it became magnetic (Z-Femag1). Notice that exposure to large volumes of air should be avoided in order to obtain highly magnetic composites. Similar magnetic composites were obtained when calcination was conducted in a nitrogen atmosphere.

In a slightly different procedure the pH of the initial 0.02 M iron salt solution was adjusted with dilute NaOH to 2.5 and stirred for 1 h at room temperature. The clear red solution (50 mL) was added to a clay suspension in water and stirred for 20 min followed by centrifugion and one washing with water. After repeating this procedure twice, the clay product was washed several times (at least nine) with water, redispersed in water, and finally dried in air for 24 h over a glass plate. The freshly prepared dry sample was subjected to the same treatment as the simply iron-exchanged sample, and the magnetic product Z-Femag2 was received.

Characterization. X-ray powder diffraction (XRD) patterns were taken on a D-500 Siemens diffractometer using the Cu Kα radiation. Infrared spectra were taken with a FT-IR spectrometer of Bruker, Equinox 55/S model. The samples were measured in the form of KBr pellets. Electron spin resonance (ESR) measurements were obtained at room temperature on a Bruker 200D-SRC spectrometer with a resonance cavity of 9.4 GHz. The Mössbauer spectra were recorded with a conventional constant acceleration spectrometer and a ^{57}Co (Rh) source. The spectra were analyzed by a least-squares fit program assuming Lorentzian line shapes. All isomer shift values are with respect to metallic iron. Magnetic measurements were carried out at room temperature in a Quantum Design Magnetometer (SQUID). TEM measurements were curried out in a JEOL JEM 2000FX electron microscope operating at 200 kV.

Results and Discussion

Characterization. The synthetic route to magnetic clays, shown schematically in Figure 1, comprises first an exchange of interlayer sodium cations for iron(III) cations (Z-Fe) with a 0.02 M $FeCl_3 \cdot 6H_2O$ aqueous solution (no pH adjustment), followed by exposure of the dried material to vapors of glacial acetic acid at 80 °C (Z-FeAc) and finally thermal treatment at 400 °C in air (Z-Femag1). For comparison, a part of the iron-exchanged sample, without the acetic acid vapors treatment, but calcined under the same conditions as the acetic acid treated product, gave a product (Z-Fe400) which did not exhibit any magnetic properties.

Figure 2 shows the XRD patterns of the samples Z-Na (a), Z-Fe (b), Z-FeAc (c), and Z-Femag1 (d). As can be seen, replacement of the sodium ions by the iron ions changes the d_{001} parameter of the parent montmorillonite from 12.5 to 14.6 Å.[21] After exposure of the Z-Fe sample to acetic acid vapors, there is an expansion of the interlayer region from 14.6 Å for the iron-saturated clay to 18 Å. In addition, we observe an improved regularity in the stacking of the individual layers, giving discernible reflections of higher order than the (001). These findings suggest that the adsorbed acetic acid vapors react with the interlayer iron centers and transform them to oligonuclear iron acetate species.[22] Subsequent calcination of the Z-FeAc sample at 400 °C leads to the magnetic composite Z-Femag1 with a totally collapsed structure (d_{001} = 9.8 Å) and an iron content of 2% measured by the 1,10-phenanthroline method.[23] The existence of magnetic γ-Fe_2O_3 particles in the final product is evidenced by the characteristic reflection at about $2\theta = 35.5°$ (inset in Figure 2). The corresponding XRD pattern of the Z-Fe calcined at 400 °C (Z-Fe400) does not show this characteristic reflection. In addition, the broaden peak at 35.5° indicates formation of nanosized particles with dimensions of about 80 Å as determined by the Scherrer equation. The acetic vapor treatment is therefore necessary for the generation of the magnetic phase. Since the XRD results of the magnetic Z-Femag1 composite indicate lack of inter-

(21) Luca, V.; Cardile, C. M. *Clays Clay Miner.* **1989**, *37*, 325.
(22) Yamanaka, S.; Hattori, M. *Catal. Today* **1988**, *2*, 261.
(23) Gerstl, Z.; Banin, A. *Clays Clay Miner.* **1980**, *28*, 335.

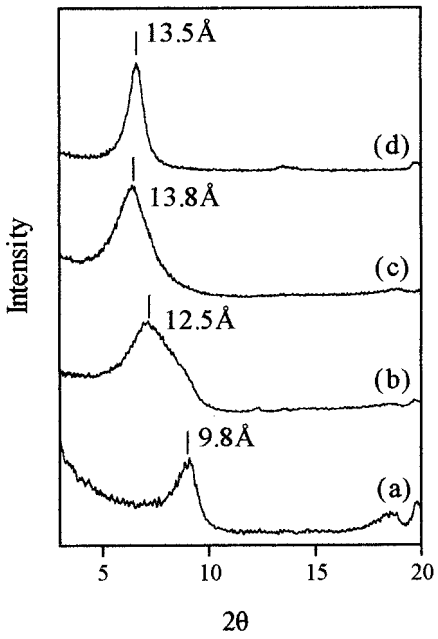

Figure 3. XRD patterns of sample Z-Femag1 (a) after aqueous exchange with Na^+ ions (b) or $(CH_3)_4N^+$ ions (c) and after vapor insertion of $(CH_3)_3N$ (d).

lamellar space, we can conclude that the iron oxide particles are dispersed on the external surfaces of the clay support with protons, fixed first in part on the clay layers during the acetic acid treatment and then during calcination, acting as balancing cations. The clay−magnetic composites retain the swelling, intercalation, and ion-exchange properties of the original montmorillonite. For instance, the magnetic composites maintain a total cation-exchange capacity near 80 mequiv/100 g as the original Na^+−montmorillonite. The protons are easily replaced by either inorganic or organic cationic species in aqueous solution through simple ion exchange or can protonate organic amines in the vapor phase, in all instances, without loss of their magnetic characteristics after drying at 80 °C. As examples to highlight these properties, the magnetic−clay composite after dispersion in water was treated with an aqueous solution of NaCl or $(CH_3)_4NCl$ for 24 h. Both treatments open up the interlamellar space of the mineral, giving the characteristic basal spacing of 12.5 and 13.8 Å, respectively (Figure 3b,c). Similarly, when trimethylamine vapors were allowed to enter the gallery space of the composite (vapor treatment at 60 °C for 24 h), protonation of the amine took place, yielding the $(CH_3)_3NH^+$−clay derivative with d_{001} = 13.5 Å (Figure 3d). These data clearly demonstrate the potential use of the Z-Femag1 composite to generate various magnetic clay derivatives. In addition to these magnetic clay derivatives, smooth and stable films can be easily produced by spreading and drying an aqueous dispersion of the magnetic clay on glass plates.

To understand and characterize better the nature of the magnetic iron oxide species and the mechanism of their interlayer formation, we present and discuss the results from FT-IR, ESR, Mössbauer, magnetic, and other measurements.

Figure 4 shows the FT-IR spectra of samples Z-Fe (b) and Z-FeAc (c) in comparison with the spectrum of trinuclear iron acetate complex $(Fe_3Ac_6O{\cdot}3H_2O)NO_3$ (a)

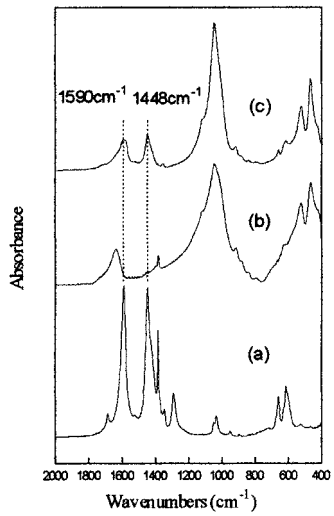

Figure 4. IR spectra of samples Z-Fe (b) and Z-FeAc (c) compared to that of trinuclear iron acetate complex (a).

prepared by a known procedure.[24] The spectrum of triacetate complex exhibits two strong absorptions at 1590 and 1448 cm^{-1}, due to the symmetric and asymmetric stretching vibrations of the $-COO^-$ bonds of acetate anion in a bridging mode of coordination.[25] As can been seen, spectrum b of the Z-Fe sample does not exhibit absorptions in these frequencies, while the same pair of peaks is clearly observed in the spectrum of Z-FeAc sample c, reflecting the presence of iron acetate species into the clay galleries. The frequency separation between these peaks, 142 cm^{-1}, is the same with that from the iron triacetate complex, suggesting that the acetic acid in the clay galleries bridges the interlayer iron centers to form small clusters that are necessary for the generation of the magnetic phase during calcination. The ability of iron acetate compounds to be transformed into crystalline magnetic phases upon pyrolysis has been reported.[26,27]

The room-temperature ESR spectrum of sodium saturated clay before the iron treatment (Z-Na) is shown in Figure 5a. The spectrum exhibits two main peaks at g = 4.3 (narrow) and g = 2.3 (broad) and one weaker at g = 9.6. The peaks at g = 4.3 and g = 9.6 arise from structural Fe^{3+} in sites of near rhombic symmetry,[21] while the broad peak at g = 2.3 can be assigned to superexchange coupling between Fe−O−Fe pairs from iron oxidic impurities dispersed on the smectite surfaces.[21] After the exchange with the iron salt (Z-Fe) a strong signal at g = 2.0 appears in the ESR spectrum (Figure 5b), which is indicative of the insertion of hydrated iron(III) species within the interlayer space of the smectite. This signal is broad because of overlap with the initial signal at g = 2.3 and also because of dipole−dipole interactions between the hydrated Fe^{3+} centers in the clay galleries. The narrowing of this signal after heating the sample at 400 °C (Figure 5c) arises from a concurrent decrease in the dipole−dipole interactions between the Fe^{3+} ions, since thermal treatment

(24) Starke, K. *J. Inorg. Nucl. Chem.* **1960**, *13*, 254.
(25) Nakamoto, K. *Infrared and Raman Spectra of Inorganic and Coordination Compounds*, 3rd ed.; Wiley-Interscience Publication: New York, 1978; p 232.
(26) Pinheiro, E. A.; Filho, P. P. A.; Galembeck, F. *Langmuir* **1987**, *3*, 445.
(27) Jewur, S. S.; Kuriacose, J. C. *Thermochim. Acta* **1977**, *19*, 195.

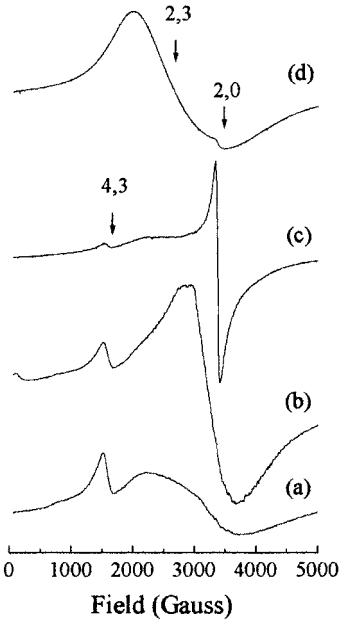

Figure 5. ESR spectra of (a) sodium saturated clay, (b) Z-Fe, (c) Z-Fe400, and (d) Z-Femag1 recorded at room temperature.

allows for the penetration of iron ions to discrete sites in the layer structure. When sample Z-Fe was exposed to acetic acid vapors and then calcined at 400 °C, the ESR spectrum changed drastically (Figure 5d). The spectrum exhibits now a weak signal at $g = 2.0$, indicating that only a small portion of Fe^{3+} ions have penetrated into the layer structure of this sample and a dominant broad signal at $g \sim 2.3$. Previous ESR studies[28] on minerals have established that iron oxide clusters on clay surfaces produce a broad signal centered around $g \sim 2.3$. Thus, the broad signal in the ESR spectrum of Z-Femag1 sample can be assigned to Fe^{3+} ions in a similar oxidic phase, in this instance magnetic oxide particles.

Figure 6 presents the ^{57}Fe Mössbauer spectra of samples Z-Fe400 recorded at L.N. (a) and Z-Femag1 at R.T. (b), L.N. (c), and L.He (d). Sample Z-Fe400 shows a paramagnetic doublet line with isomer shift $\delta = 0.46$ mm s^{-1}, relative to metallic Fe, and quadrapole splitting $\Delta = 0.88$ mm s^{-1}. Both values suggest isolated paramagnetic Fe^{3+} centers in an octahedral coordination.[21] On the other hand, sample Z-Femag1 at L.N. clearly shows, in addition to paramagnetic behavior, a magnetic hyperfine structure due to the formation of a magnetic iron oxide phase. The hyperfine field value of 519 kOe and the absence of quadrapole interactions are in line with the presence of γ-Fe_2O_3 magnetic iron oxide. The L.He spectrum displays a paramagnetic doublet (30%) and two magnetic sextets with absorption areas 30% and 40%, respectively. The first sextet has sharp lines, and its area is conserved at L.N. while at R.T. decreases to 20%. The second sextet has broad lines and at higher temperatures becomes paramagnetic. This temperature variation of the relative areas of the paramagnetic and magnetic components is typical of superparamagnetic behavior. The appearance of two magnetic components at L.He and the variation of their absorption areas above this temperature indicates the existence of at least two particle distributions: one with large particles that become superparamagnetic above L.N. and one with small particles with superparamagnetic behavior above L.He temperature. We must mention that when the nonmagnetic sample Z-Fe400 was measured at L.He, it did not reveal any magnetic hyperfine structure.

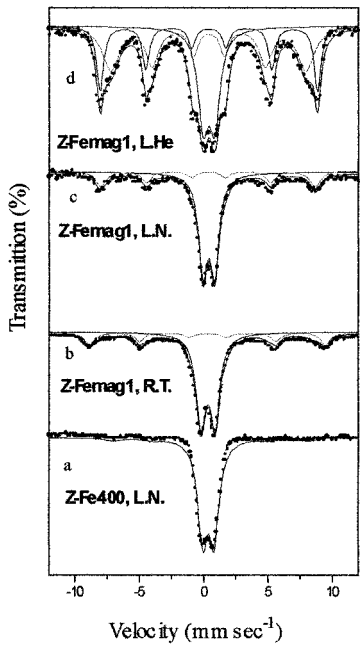

Figure 6. Mössbauer spectra of the iron-containing samples (a) Z-Fe400 recorded at 80 K, (b) Z-Femag1 recorded at room temperature, and the latter one recorded at 80 K (c) and 4.2 K (d).

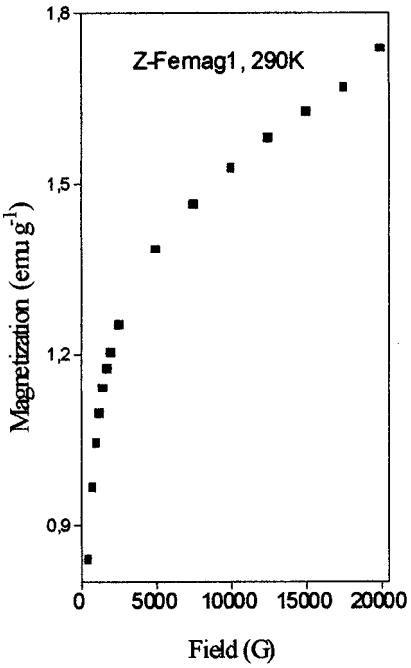

Figure 7. Magnetization curve for the sample Z-Femag1 at room temperature.

The existence of two groups of particles is also supported by SQUID magnetization measurements at room temperature (Figure 7). In the magnetization versus applied field curve we initially observe a rapid response to the applied magnetic field, attributable to large particles, and then the magnetization becomes

(28) Goodman, B. A. *Clay Miner.* **1978**, *13*, 351.

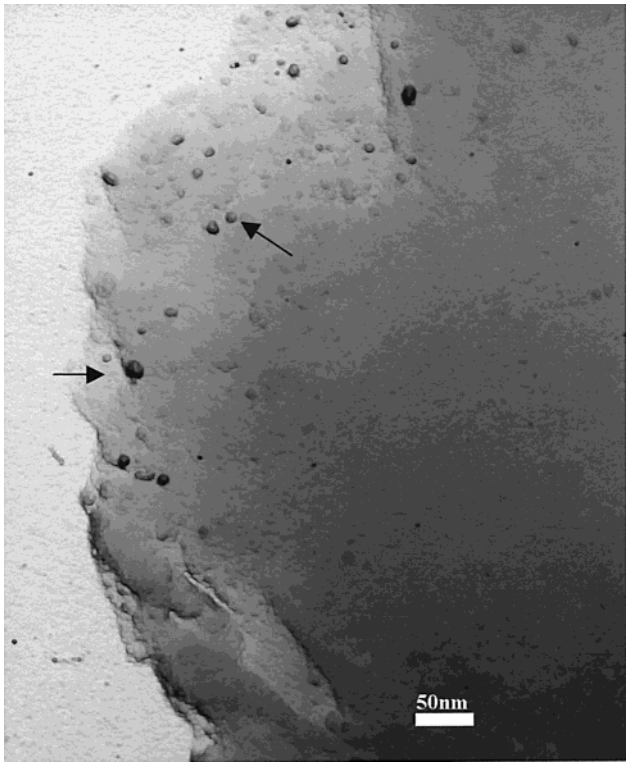

Figure 8. TEM portrait for the magnetic clay composite Z-Femag1. The arrows show representative magnetic particles over the clay surfaces.

proportional to the strength of the applied field as expected for small particles.[29] From these measurements we find that the sample Z-Femag1 possesses a magnetization of 1.75 emu g^{-1} at 2 T which remains essentially the same after any exchange process, e.g., with trimethylamine.

The morphology of the magnetic clay composite Z-Femag1 is unveiled by its TEM examination. Figure 8 displays a typical TEM portrait of the composite mineral. It appears clearly that nano γ-Fe_2O_3 particles (black spots) decorate the external surfaces of the layered support. The magnetic nanoparticles are spherical in shape and most importantly exhibit a broad particle distribution with sizes ranging between 4 and 15 nm and an average size of about 8 nm.

Synthesis of Rich Iron Magnetic Composites. The results discussed above refer to magnetic clays prepared from an iron-exchanged montmorillonite without any pH adjustment in the iron solution. If we wish to attain higher iron levels in the final product than 2%, a pH adjustment in the initial iron solution is necessary. Oligomeric iron cations were prepared by adjusting the pH of the starting solution to 2.5 by dilute NaOH. Following the same procedure as for the simple iron-exchanged sample, except for the addition of a sol instead of Fe(III) cations, we received a magnetic composite (Z-Femag2) with an iron content of 8.2%. This sample possesses increased magnetization (4.1 emu g^{-1}, 2 T) and exhibits the same features as the simply iron-saturated montmorillonite treated under the same conditions, i.e., retention of intercalation, swelling and cation-exchange properties, and stable film formation.

(29) Ida, T.; Tsuiki, H.; Ueno, A. *J. Catal.* **1987**, *106*, 428.

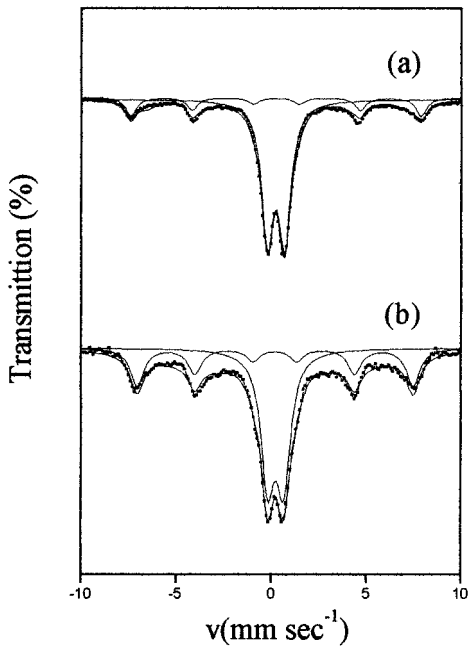

Figure 9. Mössbauer spectra of the samples Z-Femag1 (a) and Z-Femag2 (b) recorded at room temperature.

For the characterization of the Z-Femag2 nanocomposite the same techniques were employed. The FT-IR, ESR, and Mössbauer results were similar to those for the Z-Femag1 material. Thus, the IR spectra showed the characteristic absorptions at 1590 and 1448 cm^{-1}, indicating bridging of the Fe^{3+} in the assembled oligonuclear oxo complexes by the acetate groups. The ESR spectrum was dominated by a strong broad absorption at $g \sim 2.3$, consistent with nanograins of an iron oxidic phase. The Mössbauer spectra revealed superparamagnetic behavior, as the ratio of magnetic to paramagnetic area changes with the temperature of the Mössbauer measurement. An interesting result comes from the comparison of the Mössbauer spectra of the samples Z-Femag1 and Z-Femag2 recorded at room temperature (Figure 9). The ratio of the areas possessed by the magnetic components in the spectra of Z-Femag2 and Z-Femag1 was found equal to 2:1. This is in a good agreement with the ratio of the magnetization values measured for the same samples at 2 T and found equal to 2.3:1.

Conclusions

Magnetic clay composites comprised of γ-Fe_2O_3 nanoparticles immobilized onto a clay matrix, with variable iron contents up to 8.2% and magnetization values up to 4.1 emu g^{-1} (2 T), were prepared. The preparation method is based on the affinity of acetic acid vapors to react with the iron sites in an iron-exchanged montmorillonite to first form iron acetate precursor species in the interlayer space of the mineral which further produce the magnetic particles upon pyrolysis. ESR and Mössbauer results confirm the formation of γ-Fe_2O_3 nanophase particles, and XRD indicates that the γ-Fe_2O_3 nanoparticles are located outside the interlamellar space of the mineral. Strong evidence for the location of the magnetic nanoparticles in the modified clay surfaces comes from TEM which clearly shows their presence at

the external surface of the layered mineral and with particle sizes ranging between 4 and 15 nm.

The clay−γ-Fe_2O_3 composites retain the intercalation, swelling, and cation-exchange properties of the original sodium montmorillonite. The magnetic properties of the composites remain unchanged after any desirable modification to generate several reconstructed clay derivatives. Additionally, these novel materials are easily redispersed in water and upon drying form stable magnetic films. These important properties offer potential new aspects for clay particle engineering applications (films), intercalation chemistry, and industrial utilities (fillers).

CM000137O